nature photonics

LETTERS

PUBLISHED ONLINE: 23 MAY 2010 | DOI: 10.1038/NPHOTON.2010.119

# Mid-infrared optical parametric amplifier using silicon nanophotonic waveguides

Xiaoping Liu[1], Richard M. Osgood Jr[1], Yurii A. Vlasov[2] and William M. J. Green[2]*

**All-optical signal processing is an approach used to dramatically decrease power consumption and speed up the performance of next-generation optical telecommunications networks[1–3]. Nonlinear optical effects such as four-wave mixing and parametric gain have been explored to realize all-optical functions in glass fibres[4]. An alternative approach is to use nanoscale engineering of silicon waveguides to enhance optical nonlinearities by up to five orders of magnitude[5], enabling integrated chip-scale all-optical signal processing. Four-wave mixing within silicon nanophotonic waveguides has been used to demonstrate telecom-band ($\lambda \approx 1{,}550$ nm) all-optical functions including wavelength conversion[6–9], signal regeneration[10] and tunable optical delay[11]. Despite these important advances, strong two-photon absorption[12] of the telecom-band pump presents a fundamental obstacle, limiting parametric gain to values of several decibels[13]. Here, we demonstrate a silicon nanophotonic optical parametric amplifier exhibiting broadband gain as high as 25.4 dB, using a mid-infrared pump near one-half the bandgap energy ($E \approx 0.55$ eV, $\lambda \approx 2{,}200$ nm), where parasitic two-photon absorption-related absorption vanishes[12,14,15]. This gain is high enough to compensate all insertion losses, resulting in 13-dB net off-chip amplification, using only an ultra-compact 4-mm silicon chip. Furthermore, engineering of higher-order waveguide dispersion[16] can potentially enable mid-infrared-pumped silicon parametric oscillators[17–19] and amplifiers for telecom-band optical signals.**

Going beyond its significant relevance to the field of all-optical signal processing, the broadband parametric amplifier demonstrated here also facilitates the simultaneous generation of multiple on-chip mid-infrared sources through cascaded four-wave mixing (FWM), covering a 500-nm spectral range. Together, these results provide a foundation for the construction of silicon-based room-temperature mid-infrared light sources including tunable chip-scale optical-frequency combs[20] and supercontinuum generators[21]. In this manner, silicon nanophotonic technology may be extended to an entirely new class of mid-infrared applications[22–24], including biochemical detection, environmental monitoring and free-space communication, for which an integrated on-chip platform can be of great benefit.

To achieve large, broadband nonlinear parametric gain in silicon, the FWM process[25] relies upon precise phase matching between the co-propagating pump, signal and idler waves, as well as the presence of a strong nonlinear interaction, described by the effective nonlinearity parameter $\gamma$. In addition, the intrinsic nonlinear figure of merit (FOM) of silicon is $n_2/(\beta_{\mathrm{TPA}} \cdot \lambda)$, where $n_2$ is the intensity-dependent refractive index and $\beta_{\mathrm{TPA}}$ is the two-photon absorption (TPA) coefficient. Ideally, FOM should be as large as possible. Although a large TPA coefficient restricts FOM to values less than 0.4 near $\lambda = 1{,}550$ nm, at mid-infrared wavelengths approaching the TPA threshold of silicon at $\lambda \approx 2{,}200$ nm, the FOM can increase by as much as a factor of ten to FOM $> 4$. The mid-infrared is therefore a highly promising spectrum for realizing chip-scale silicon nanophotonic all-optical devices for which the performance is no longer restricted by parasitic nonlinear absorption.

The essential dispersion and nonlinearity characteristics for a mid-infrared silicon nanophotonic waveguide were engineered through a comprehensive multi-parameter design-space study, encompassing the nanoscale silicon core dimensions, the cladding refractive index and the waveguide mode polarization (see Supplementary Information). The resulting geometry ultimately selected for fabrication is shown in the scanning electron microscopy (SEM) cross-sectional image in Fig. 1a. The silicon waveguide core has dimensions of 700 nm $\times$ 425 nm, and is designed to operate in the fundamental quasi-transverse magnetic (TM) mode near $\lambda = 2{,}200$ nm, as illustrated by the overlaid mode field profile. The nanoscale-engineered optical structure is precisely controlled using a combination of silicon epitaxy, deep-ultraviolet lithography, reactive ion etching and dielectric deposition, within an advanced complementary metal-oxide-semiconductor (CMOS) fabrication facility (see Supplementary Information).

The calculated dispersion coefficient $D$ and effective nonlinearity parameter $\gamma$ for this specific silicon nanophotonic waveguide configuration are plotted in Fig. 1b, illustrating the mid-infrared spectral dependence near the TPA threshold of silicon. The dispersion is designed to be zero at a wavelength of $\lambda = 2{,}260$ nm. The pump wavelength is chosen to be $\lambda = 2{,}170$ nm so that the nanophotonic waveguide has anomalous dispersion conditions with $D = 1{,}000$ ps nm$^{-1}$ km$^{-1}$, as required for broadband phase matching[25]. Strong optical confinement of the quasi-TM mode to the $\sim$0.3-$\mu$m$^2$ silicon core results in a large effective nonlinearity of $\gamma = 110$ W$^{-1}$ m$^{-1}$ at $\lambda = 2{,}170$ nm, a value more than ten times larger than that of planar chalcogenide glass waveguides[26], and four orders of magnitude larger than that of highly nonlinear optical fibre[4,27].

The mid-infrared nonlinear characteristics of a 4-mm-long silicon nanophotonic waveguide were studied by simultaneously injecting picosecond pump pulses centred at $\lambda = 2{,}170$ nm together with a continuous-wave (c.w.) tunable mid-infrared laser signal, and observing the resulting FWM at the waveguide output (for experimental details see Methods). The peak coupled pump power at the waveguide input was $P_{\mathrm{p}} \approx 27.9$ W, and the input signal power $P_{\mathrm{sig}}$ was kept below 0.45 mW. For each spectrum shown in Fig. 1c, two photons from the high-intensity pulsed pump mix with a single photon from the tunable c.w. signal to generate a wavelength-converted idler photon, at a wavelength dictated by energy conservation[25]. The FWM process also produces an additional photon at the signal wavelength, which can ultimately contribute to signal amplification. Owing to the pulsed nature of the pump, the generated idler and amplified signals also occur as short pulses.

[1]Department of Electrical Engineering, Columbia University, 1300 S.W. Mudd Building, 500 W. 120th Street, New York, New York 10027, USA, [2]IBM Thomas J. Watson Research Center, Yorktown Heights, New York 10598, USA. *e-mail: wgreen@us.ibm.com

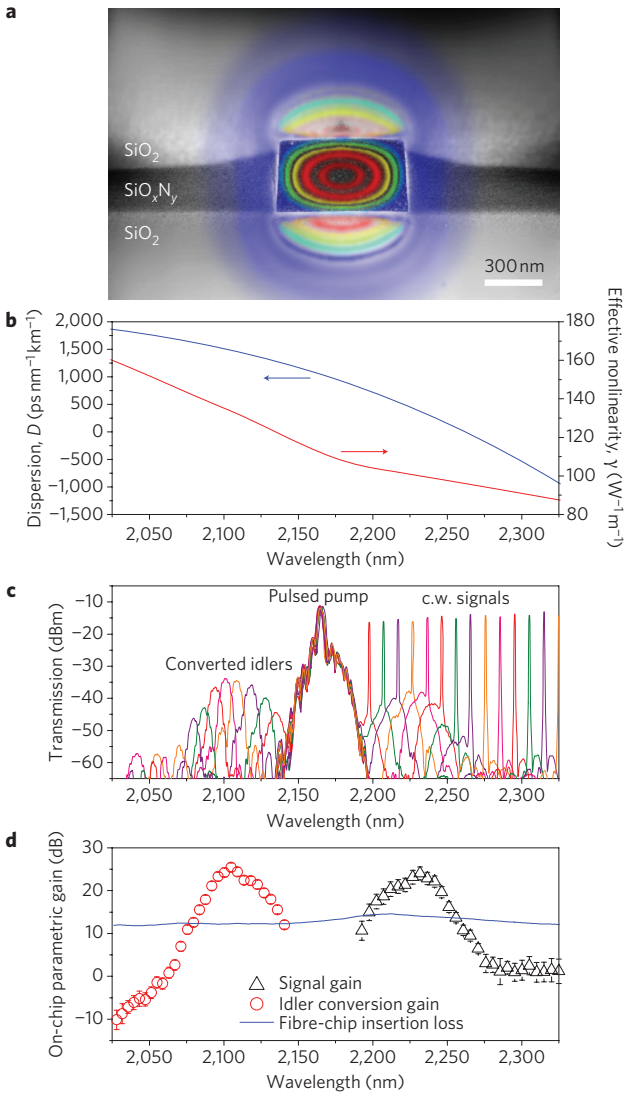


**Figure 1 | Engineered silicon nanophotonic waveguide characteristics, mid-infrared FWM experiments and broadband on-chip optical parametric amplification. a**, SEM cross-section of the 700 nm × 425 nm silicon waveguide. The colour-map illustrates the $E_y$ component of the fundamental quasi-TM mode at $\lambda = 2{,}200$ nm. **b**, Simulated dispersion coefficient $D$ (blue curve) and effective nonlinearity parameter $\gamma$ (red curve). **c**, Series of FWM spectra taken at the output of the 4-mm-long waveguide. **d**, On-chip parametric signal gain (black triangles) and idler conversion gain (red circles), with bandwidth of ~220 nm and peak values >25 dB. Net off-chip gain results where amplification exceeds fibre-chip insertion losses (blue line), with a maximum value of ~13 dB. Estimation of error bars is described in Supplementary Information.

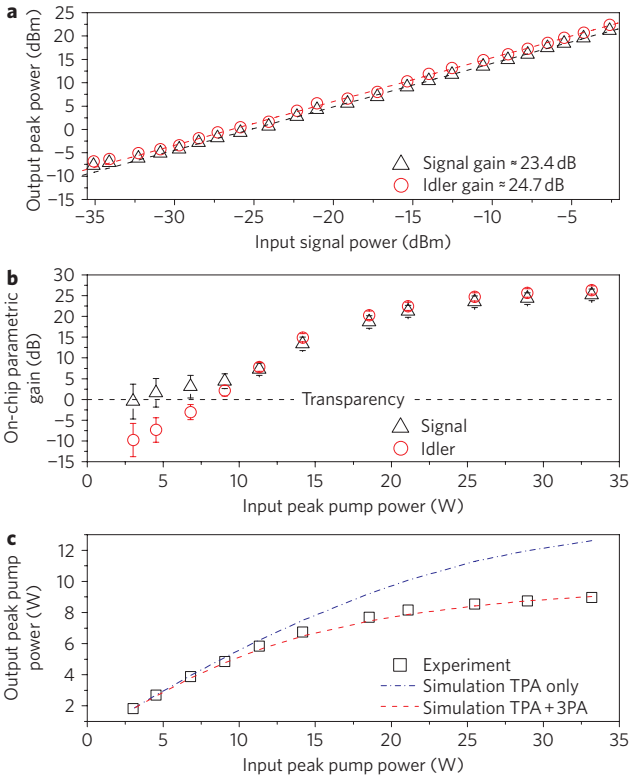


**Figure 2 | Mid-infrared optical parametric amplifier performance characteristics. a**, Output peak signal/idler power versus input signal power at $\lambda = 2{,}238$ nm and peak pump power $P_p \approx 27.9$ W. Measurements show a linear amplifier response over a dynamic range >30 dB. **b**, On-chip signal/idler gain versus input peak pump power, input signal power $P_{sig} \approx 0.39$ mW at $\lambda = 2{,}238$ nm. Transparency was reached at $P_p \approx 7.5$ W. **c**, Output peak pump power versus input peak pump power. Experimentally measured data points are shown by black squares. The blue dash – dotted and red dashed curves illustrate simulated transmission models accounting for nonlinear loss from TPA only and TPA-plus-3PA, respectively.

The FWM spectra in Fig. 1c were analysed to extract the on-chip parametric signal gain and idler conversion gain values plotted in Fig. 1d (see Methods). The experimental data reveal that the engineered silicon nanophotonic waveguide successfully functions as a mid-infrared optical parametric amplifier (OPA), with very large maximum signal and idler gain values of 24 and 25.4 dB, respectively. Moreover, the on-chip parametric gain is significant enough to overcome substantial fibre-chip coupling losses (blue curve), demonstrating net off-chip gain as large as 10 dB for the signal and 13 dB for the idler. The overall on-chip gain bandwidth spans the range from 2,060 to 2,280 nm, with the two prominent gain peaks coinciding with the envelopes of the pulsed signal and idler spectra in Fig. 1c. The maximum parametric gain obtained using our ultra-compact 4-mm device was more than 100 times larger than that previously observed in a 17-mm-long silicon waveguide pumped near $\lambda = 1{,}550$ nm, where gain was limited to ~3 dB because of strong TPA-induced saturation effects[13]. By operating the pump at longer wavelengths in the mid-infrared, we have realized a chip-scale silicon nanophotonic OPA that breaks the limits set by TPA nonlinear absorption.

Additional experiments were carried out with the input signal tuned to the gain peak at $\lambda = 2{,}238$ nm to thoroughly characterize the OPA input – output and gain saturation characteristics. Figure 2a plots the output peak signal and idler power versus input signal power, with pump power $P_p \approx 27.9$ W. The dashed fit lines highlight linear amplification over a dynamic range significantly larger than 30 dB, with signal and idler gains of 23.4 dB and 24.7 dB, respectively. Figure 2b plots on-chip signal/idler gain versus input pump power, with signal power $P_{sig} \approx 0.39$ mW. The intersection with the dotted line illustrates that on-chip transparency is reached with a pump power near $P_p \approx 7.5$ W. These pump requirements may be reduced by increasing the waveguide length, or by suitable nanoscale engineering of the waveguide cross-section to increase the effective nonlinearity. Figure 2b also shows that saturation does not begin until $P_p \approx 19$ W, at which point signal and idler gain both exceed 20 dB. The measurements reveal that this gain saturation is strongly correlated with self-limiting of the transmitted pump power, as shown by the black open

squares in Fig. 2c. Numerical models used to assess the origin of this self-limiting (see Methods) reveal that a residual TPA coefficient[15] of $\beta_{TPA} = 0.106$ cm GW$^{-1}$ cannot alone account for the observed saturation at high input pump power (blue dash–dotted curve). The significantly reduced value of $\beta_{TPA}$ at $\lambda = 2{,}170$ nm, approximately seven times smaller than at $\lambda = 1{,}550$ nm, suggests that higher-order nonlinear absorption dominates under these OPA operating conditions. The red dashed curve in Fig. 2c shows that when a three-photon absorption (3PA) coefficient[28] of $\gamma_{3PA} = 0.025$ cm$^3$ GW$^{-2}$ is included in the simulation together with TPA, the model accurately predicts the experimental trend. However, even though 3PA is expected to play a role up to $\lambda \approx 3{,}300$ nm, the characteristics of the OPA demonstrated here clearly illustrate that nonlinear absorption no longer presents a significant obstacle to obtaining parametric gain large enough for practical applications in all-optical signal processing[1–3].

The large on-chip parametric gain produces amplified picosecond signal and idler pulses having a peak power of several hundred milliwatts within the silicon nanophotonic OPA, which can themselves mix with the pump to efficiently generate new wavelengths through cascaded FWM. As shown by the spectrum in Fig. 3, four orders of cascaded mixing products (numbered peaks 3–9) spanning a spectral bandwidth of 500 nm are observed when the pump (peak 1) is operated at $\lambda = 2{,}180$ nm ($P_p \approx 21.8$ W), and the signal (peak 2) is tuned to $\lambda = 2{,}240$ nm with an increased input power of $P_{sig} \approx 4.4$ mW. Although on-chip parametric gain under these conditions is restricted to the spectral range $2{,}086\text{ nm} < \lambda < 2{,}273$ nm (hatched region), an analysis of the wavelength conversion efficiency at each cascaded mixing peak can assist in further quantifying the OPA characteristics within the regions that experience no gain. For example, the various FWM combinations that can give rise to peak 5 are listed in Table 1. As depicted by the inset energy diagram in Fig. 3, the most sensible dominant term originates from non-degenerate FWM of peaks 1 and 3 as pumps, leading to wavelength conversion of a signal at peak 4 into an idler at peak 5. The conversion efficiency for this mixing term is approximately −12 dB. Applying a similar approach, the conversion efficiencies for peaks 6–9 range from −4 to −9 dB, values approximately 8–10 dB larger than those observed in recent silicon mid-infrared wavelength conversion experiments[29,30]. These results illustrate that even far outside the parametric gain bandwidth, the present silicon nanophotonic OPA design can be used as a power-efficient generator of broadband mid-infrared white light and/or multi-line sources.

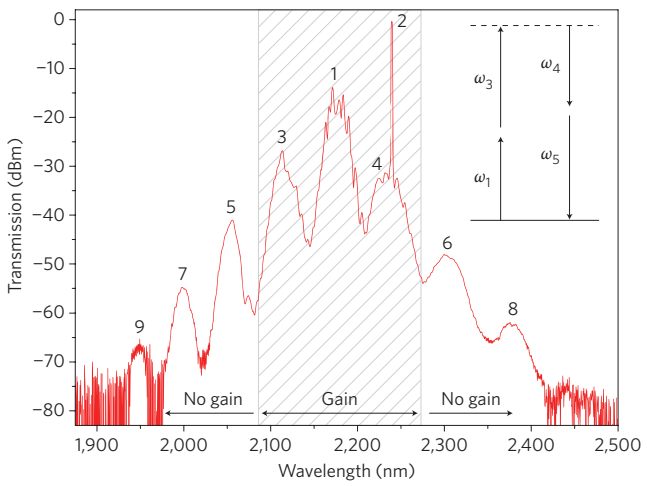


**Figure 3 | Broadband mid-infrared light generation by efficient cascaded FWM.** Transmission spectrum illustrating four orders of cascaded mixing products at the silicon nanophotonic OPA output, covering a total bandwidth of 500 nm. The hatched spectral region $2{,}086\text{ nm} < \lambda < 2{,}273$ nm experiences on-chip parametric gain, and net on-chip loss is observed outside this region. The inset energy diagram illustrates the dominant FWM process contributing to peak 5.

**Table 1 | Mixing terms contributing to peak 5 of the cascaded FWM spectrum shown in Fig. 3.**

| Mixing combination (idler: pump 1, pump 2, signal) | Effective pump power (dBm) | Signal power (dBm) | Idler power (dBm) | Conversion efficiency (dB) |
|---|---|---|---|---|
| 5:3,1,4 | 32.1 | 23.7 | 11.2 | −12.5 |
| 5:3,3,1 | 25.6 | 38.5 | 11.2 | −27.3 |
| 5:3,1,2 | 32.1 | 3.7 | 11.2 | 7.5 |
| 5:1,1,6 | 38.5 | 7.2 | 11.2 | 4.0 |
| 5:1,4,8 | 31.1 | −6.2 | 11.2 | 17.4 |

Possible FWM combinations are labelled according to the role of each numbered peak in the FWM process. The power in each peak is evaluated as described in the Methods. The effective pump power is given by $\sqrt{(P_{pump1}P_{pump2})}$. The conversion efficiency is defined as the ratio of idler and signal power, $P_{idler}/P_{signal}$. Mixing terms that suggest a conversion efficiency greater than zero, that is, idler conversion gain, are ruled out by the fact that peak 5 lies outside the experimentally determined gain bandwidth. The dominant source for peak 5 probably originates from the remaining combination with the largest effective pump power, that is, combination 5:3,1,4.

Taken together, the results above provide strong encouragement for a broad extension of the capabilities of the integrated silicon nanophotonic platform into the mid-infrared spectrum. Making use of the ultra-compact high-gain OPA demonstrated here, a direction of immediate interest is the introduction of resonant feedback to develop a silicon-based, low-threshold, highly portable optical parametric oscillator[17] (OPO). Novel broadband room-temperature light sources such as these would have wide-ranging applications in mid-infrared spectroscopy, sensing and free-space communication[22–24].

## Methods

**Waveguide characterization and FWM measurements.** Silicon nanophotonic waveguide propagation losses near $\lambda = 2{,}200$ nm were measured using the cutback method, by measuring transmission of broadband amplified spontaneous emission (ASE) from the tunable mid-infrared c.w. laser (Photonics Innovations SFTL; $Cr^{2+}$:ZnSe polycrystal with erbium-fibre laser pump source) through waveguides having various lengths from 4 to 45 mm. Unpolarized emission from the laser operating below threshold was coupled into a single-mode fibre using a microscope objective and micropositioner stage. Lensed tapered fibres were aligned to the silicon nanophotonic waveguide facets with $x$–$y$–$z$ piezoelectric positioners for on-/off-chip coupling. Transmission spectra at the waveguide output were characterized with a mid-infrared optical spectrum analyser (Yokogawa AQ6375) operating at 1-nm resolution bandwidth. The propagation loss varied from ~4 dB cm$^{-1}$ at 2,030 nm to 10 dB cm$^{-1}$ at 2,500 nm, with an uncertainty of ±2.5 dB cm$^{-1}$. The increased propagation losses at longer wavelengths were probably due to elevated optical absorption in the silica waveguide cladding materials[22]. Subtracting the linear propagation loss from the total measured fibre-to-fibre insertion loss, a coupling loss from the lensed fibre into the silicon nanophotonic waveguide of ~6.5±1 dB/facet was estimated.

For the FWM experiments, collimated beams from the mid-infrared picosecond pulsed pump (mode-locked Ti:sapphire-pumped Coherent Mira-OPO system, full-width at half-maximum (FWHM) ≈ 2 ps, repetition rate = 76 MHz) and c.w. tunable signal lasers first passed through variable neutral density filters for power control, and were then coupled into separate single-mode fibres. The pump and signal were multiplexed using a fused fibre directional coupler (99:1 ratio for parametric gain measurements, 90:10 ratio for cascaded FWM measurements). The combined optical power was coupled into a 4-mm-long waveguide using lensed tapered fibres. Polarization controllers were used to co-polarize both pump and signal to selectively excite the fundamental quasi-TM waveguide mode.

**Extraction of parametric conversion efficiency and signal gain.** The peak power of the converted idler pulse at the output of the silicon nanophotonic waveguide, $P_{idler\_out}$, was derived from the measured FWM spectra according to $P_{idler\_out} = F(\int P_{idler\_avg}(\lambda)d\lambda)$. To convert the time-averaged idler power $P_{idler\_avg}$ measured by the OSA into peak power, the spectrally integrated power was weighted by the duty cycle factor $F = 1/(76\text{ MHz} \cdot 2\text{ ps})$, due to the pulsed nature of the experiment. A similar procedure was applied to find the pulsed signal output power $P_{signal\_out}$. A 2-nm-wide band-stop filter was first numerically applied to the time-averaged signal spectrum to (conservatively) exclude the power remaining

in the narrowband c.w. tone. The peak signal power was then computed according to $P_{signal\_out} = F(\int P_{signal\_filtered\_avg}(\lambda)d\lambda)$. Finally, to find the c.w. signal power at the waveguide input $P_{signal\_in}$, the output c.w. signal power was measured (with the pump off) and corrected to account for total propagation losses of $\alpha$ dB incurred through the 4-mm-long device, $P_{signal\_in} = 10^{\alpha/10}(\int P_{signal\_out\_pump\_off}(\lambda)d\lambda)$. Using the above quantities, the on-chip idler conversion gain $\eta$ was then defined as the ratio of peak idler power and input c.w. signal power, $\eta = P_{idler\_out}/P_{signal\_in}$. Accordingly, on-chip signal gain was given by $G = P_{signal\_out}/P_{signal\_in}$. The error bars in the on-chip parametric gain data are derived from the uncertainty in the total propagation loss $\alpha$, as well as the contribution of the OSA noise floor accumulated when integrating the signal/idler power at the waveguide output. Additional details on the estimation of error bars are included in the Supplementary Information.

**Numerical simulations of pulse propagation and TPA/3PA coefficient fitting.** A perturbed nonlinear Schrödinger equation (NLSE) model[5] was used to simulate the pulse dynamics in the silicon nanophotonic waveguide. The underlying NLSE was solved with a split-step Fourier transform technique, in which the linear part of the NLSE was solved in the Fourier domain, and the nonlinear part was solved in the time domain with a fourth-order Runge–Kutta method. Nonlinear loss mechanisms including TPA, 3PA and related free-carrier absorption (FCA) were taken into account. The TPA and 3PA coefficients were varied within the range of experimental uncertainty in the bulk silicon data[15,28] to best fit the measured pump self-limiting curve. All other parameters, including waveguide dispersion, effective nonlinearity, propagation loss and input power, were matched to the corresponding experimental conditions.

Received 11 January 2010; accepted 2 April 2010; published online 23 May 2010

## References


1. Tucker, R. S. The role of optics and electronics in high-capacity routers. *J. Lightwave Technol.* **24,** 4655–4673 (2006).
2. Blumenthal, D. J., Prucnal, P. R. & Sauer, J. R. Photonic packet switches: architectures and experimental implementations. *Proc. IEEE* **82,** 1650–1667 (1994).
3. Cotter, D. *et al.* Nonlinear optics for high-speed digital information processing. *Science* **286,** 1523–1528 (1999).
4. Radic, S. & McKinstrie, C. J. Optical amplification and signal processing in highly nonlinear optical fiber. *IEICE Trans. Electron.* **E88-C,** 859–869 (2005).
5. Dadap, J. I. *et al.* Nonlinear-optical phase modification in dispersion-engineered Si photonic wires. *Opt. Express* **16,** 1280–1299 (2008).
6. Claps, R., Raghunathan, V., Dimitropoulos, D. & Jalali, B. Anti-Stokes Raman conversion in silicon waveguides. *Opt. Express* **11,** 2862–2872 (2003).
7. Espinola, R. L., Dadap, J. I., Osgood, R. M. Jr, McNab, S. J. & Vlasov, Y. A. C-band wavelength conversion in silicon photonic wire waveguides. *Opt. Express* **13,** 4341–4349 (2005).
8. Fukuda, H. *et al.* Four-wave mixing in silicon wire waveguides. *Opt. Express* **13,** 4629–4637 (2005).
9. Rong, H., Kuo, Y.-H., Liu, A., Paniccia, M. & Cohen, O. High efficiency wavelength conversion of 10 Gb $s^{-1}$ data in silicon waveguides. *Opt. Express* **14,** 1182–1188 (2006).
10. Salem, R. *et al.* Signal regeneration using low-power four-wave mixing on silicon chip. *Nature Photon.* **2,** 35–38 (2008).
11. Dai, Y. *et al.* 1 μs tunable delay using parametric mixing and optical phase conjugation in Si waveguides. *Opt. Express* **17,** 7004–7010 (2009).
12. Raghunathan, V., Shori, R., Stafsudd, O. & Jalali, B. Nonlinear absorption in silicon and the prospects of mid-infrared silicon Raman lasers. *Phys. Status Solidi A* **203,** R38–R40 (2006).
13. Foster, M. A. *et al.* Broad-band optical parametric gain on a silicon photonic chip. *Nature* **441,** 960–963 (2006).
14. Jalali, B. *et al.* Prospects for silicon mid-IR Raman lasers. *IEEE J. Sel. Top. Quantum Electron.* **12,** 1618–1627 (2006).
15. Bristow, A. D., Rotenberg, N. & van Driel, H. M. Two-photon absorption and Kerr coefficients of silicon for 850–2,200 nm. *Appl. Phys. Lett.* **90,** 191104 (2007).
16. Dulkeith, E., Xia, F., Schares, L., Green, W. M. J. & Vlasov, Y. A. Group index and group velocity dispersion in silicon-on-insulator photonic wires. *Opt. Express* **14,** 3853–3863 (2006).
17. Lin, Q., Johnson, T. J., Perahia, R., Michael, C. P. & Painter, O. J. A proposal for highly tunable optical parametric oscillation in silicon micro-resonators. *Opt. Express* **16,** 10596–10610 (2008).
18. Levy, J. S. *et al.* CMOS-compatible multiple-wavelength oscillator for on-chip optical interconnects. *Nature Photon.* **4,** 37–40 (2010).
19. Razzari, L. *et al.* CMOS compatible integrated optical hyper-parametric oscillator. *Nature Photon.* **4,** 41–45 (2010).
20. Del'Haye, P. *et al.* Optical frequency comb generation from a monolithic microresonator. *Nature* **450,** 1214–1217 (2007).
21. Hsieh, I.-W. *et al.* Supercontinuum generation in silicon photonic wires. *Opt. Express* **15,** 15242–15249 (2007).
22. Soref, R. A., Emelett, S. J. & Buchwald, W. R. Silicon waveguided components for the long-wave infrared region. *J. Opt. A* **8,** 840–848 (2006).
23. Soref, R. Towards silicon-based longwave integrated optoelectronics (LIO). *Proc. SPIE* **6898,** 5 (2008).
24. Ebrahim-Zadeh, M. & Sorokina, I. T. *Mid-Infrared Coherent Sources and Applications* 1st edn (Springer, 2007).
25. Agrawal, G. P. *Nonlinear Fiber Optics* 3rd edn (Academic Press, 2001).
26. Lamont, M. R. E., de Sterke, C. M. & Eggleton, B. J. Dispersion engineering of highly nonlinear $As_2S_3$ waveguides for parametric gain and wavelength conversion. *Opt. Express* **15,** 9458–9463 (2007).
27. Chavez-Boggio, J. M. *et al.* 730-nm optical parametric conversion from near- to short-wave infrared band. *Opt. Express* **16,** 5435–5443 (2008).
28. Pearl, S., Rotenberg, N. & van Driel, H. M. Three photon absorption in silicon for 2,300−3,300 nm. *Appl. Phys. Lett.* **93,** 131102 (2008).
29. Turner-Foster, A. C., Foster, M. A., Salem, R., Gaeta, A. L. & Lipson, M. Frequency conversion in silicon waveguides over two-thirds of an octave. *Proceedings of the Conference on Lasers and Electro-Optics/International Quantum Electronics Conference*, CFR4 (2009).
30. Park, J. S. *et al.* Mid-infrared four-wave mixing in silicon waveguides using telecom-compatible light sources. *Proceedings of Frontiers in Optics*, PDPB3 (2009).


## Acknowledgements

The authors gratefully acknowledge help from the staff at the IBM Microelectronics Research Laboratory where the silicon nanophotonic OPA devices were fabricated, K. Reuter and B. Price for assistance with SEM images, and J. Dadap for assistance with optimization of the pulsed laser system used in the experiments. Thanks also go to T. Kippenberg, G. Roelkens, R. Soref, S. Assefa and J. Van Campenhout for many helpful and motivating discussions.

## Author contributions

W.M.J.G. conceived and supervised the experiments, and developed the device fabrication process. X.L. performed the numerical dispersion engineering, effective nonlinearity and nonlinear pulse propagation calculations, under the supervision of R.M.O. X.L. and W.M.J.G. jointly designed the mid-infrared waveguide dimensions and performed the experiments. X.L., R.M.O., Y.A.V. and W.M.J.G. all contributed to the data analysis and writing of the manuscript.

## Additional information

The authors declare no competing financial interests. Supplementary information accompanies this paper at www.nature.com/naturephotonics. Reprints and permission information is available online at http://npg.nature.com/reprintsandpermissions/. Correspondence and requests for materials should be addressed to W.M.J.G.